Enhanced Pool-Boiling Heat Transfer and Critical Heat Flux Using Femtosecond Laser Surface Processing

Corey M. Kruse[1], Troy Anderson[2], Chris Wilson[2], Craig Zuhlke[2], Dennis Alexander[2], George Gogos[1], Sidy Ndao*[1]
University of Nebraska - Lincoln,
[1]Mechanical and Materials Engineering
[2]Electrical Engineering
Lincoln, Nebraska, U.S., 68588
Email: sndao2@unl.edu

ABSTRACT

In this paper, we present the experimental investigation of pool boiling heat transfer on multiscale (micro/nano) functionalized metallic surfaces. The microstructures used in the experiments were fabricated via a femtosecond laser surface process (FLSP) technique which forms mound-like microstructures covered by layers of nanoparticles. Using a pool boiling experimental setup with deionized water as the working fluid, both the heat transfer coefficients and critical heat flux were investigated. The polished reference sample was found to have a critical heat flux of 91 W/cm2 at 39.8 °C of superheat and a maximum heat transfer coefficient of 23,000 W/m2C. The processed sample was found to have a critical heat flux of 122 W/cm2 with 18.1 ºC superheat and a maximum heat transfer coefficient of 67,400 W/m2C. Flow visualization revealed nucleate boiling to be the main two-phase heat transfer mechanism. The overall heat transfer performance of the metallic multiscale structured surface has been attributed to both augmented heat transfer surface area and enhanced nucleate boiling regime. On the other hand, increase in the critical heat flux can be attributed to the superhydrophilic nature of the laser processed surfaces and the presence of nanoparticle layers.

KEY WORDS: Pool Boiling, Critical Heat Flux, Femtosecond Laser Surface Processing, Multiscale Surfaces, Metallic Surface Enhancement

INTRODUCTION

Two-phase heat transfer on micro and nanostructured surfaces has attracted much research interest in recent time. This is due to the observed high heat transfer coefficients and critical heat flux. Most pool boiling experiments for enhanced heat transfer have been conducted on micro and nanostructured surfaces fabricated using complex fabrication techniques such as etching and film depositions carried out in highly controlled environments (i.e., cleanroom). These techniques have been very effective at increasing the critical heat flux (CHF) as well as the heat transfer coefficient (HTC). These techniques enhance the CHF and HTC by a combination of increasing surface roughness, wettability, and porosity. These microfabrication techniques have been used to create very organized arrays of microstructures ranging from pillars to microchannels. These structures have demonstrated CHF values of around 150 – 200 W/cm^2 [1], [2] for pillars and 100 W/cm^2 [3] for microchannels. When nanoscale features are added to these microstructures the critical heat flux is increased to around 230 W/cm^2 for the pillar structure [1] and around 160 W/cm^2 for the microchannels with nanostructures [3]. This shows that the addition of a hierarchical structure can significantly increase the performance of a surface. It has also been shown that a combination or network of hydrophilic and hydrophobic areas on a boiling surface can significantly enhance the performance as well. The hydrophobic areas lead to easily activated nucleation sites while the hydrophilic areas prevent the vapor from forming a stable layer and thus delaying the critical heat flux [4], [5].

In addition to the organized arrays of microstructures, these traditional microfabrication techniques have also been used to fabricate silicon and copper nanowires that coat the boiling surface. These types of surfaces have been shown to produce CHF values in the range of 120-200 W/cm^2 [6]–[8]. All of these CHF enhancements are typically attributed to high nucleation density, superhydrophilicity, and enhanced capillary pumping. All the previously mentioned experimental results were conducted with a heat transfer surfaced comprised of a silicon base material. This type of surface is advantageous in small applications, like electronic devices, that use silicon regularly. These types of surface enhancement techniques are not practical for applications which require metallic heat transfer surfaces and much larger areas.

Some work has been done to enhance heat transfer surfaces with a metallic base. These enhancement methods involve an oxidation processes or material deposition to achieve the desired micro/nanostructures. These methods are also typically limited to a certain type base material. Through the use of an anodic oxidation process on a zirconium alloy, a CHF of around 200 W/cm^2 can be reached [9]. This process results in random pyramid microstructures with a nanoscale roughness. In other work, alumina was deposited onto platinum using atomic layer deposition [10] and zinc oxide was deposited onto copper and aluminum surfaces in order to enhance the surface [11]. The alumina deposition on platinum resulted in a CHF of around 120 W/cm^2 while the zinc oxide covered surfaced only reached maximum heat fluxes of around 65 W/cm^2.

Our current research focuses on using a technique referred to as Femtosecond Laser Surface Processing (FLSP). This technique uses and ultra-fast laser to ablate and form a self-organized array of mound like microstructures with a nanoparticle layer on any metallic surface. This method is a one step process that has the advantage of being able to process nearly any size of area with a very high precision. This technique was used to enhance the heat transfer properties of a stainless steel surface used in pool boiling two phase heat transfer.

EXPERIMENTAL PROCEDURES

Laser Manufacturing

Multiscale surfaces (surfaces with roughness on both the micrometer and nanometer scales) are commonly applied for the fabrication of advanced wettability surfaces that range from superhydrophobic to superhydrophilic [12]–[17]. Indeed, such surfaces are considered to be biologically inspired as they often mimic the surfaces of plant leaves; one iconic example is the superhydrophobic lotus leaf, which exhibits self-cleaning properties due in part to multiscale surface features [18], [19] . For such structured surfaces, the relative sizes of both micrometer and nanometer scale structures are critical for the control of not only the contact angle, but also the adhesion and wetting state (e.g. the fully-wetting Wenzel state or the hybrid Cassie-Baxter state) [19].

Femtosecond laser surface processing (FLSP) is rapidly emerging as a powerful and dynamic method for the fabrication of biologically inspired multiscale surface structures. Using this process, surfaces generally consist of self-organized, quasi-periodic micron-scale conical or mound structures that are covered in a layer of nanoparticles [20]–[27]. These surface structures are formed through a complex combination of multiple growth mechanisms including laser ablation, capillary flow of laser-induced melt layers, and redeposition of ablated material.

A schematic of the FLSP setup is shown in Figure 1. The laser was a Ti:Sapphire (Spitfire, Spectra Physics) that produced ~50 femtosecond pulses centered around 800 nm at a 1 kHz repetition rate. The laser power was controlled through a combination of a half waveplate and a polarizer. A refractive Gauss-to-top hat beam shaper (Eksma Optics, GTH-4-2.2FA) was used to generate a top hat beam with a square profile; this ensured that the laser fluence on the sample was uniform. The sample was placed on a computer-controlled 3D translation stage and translated through the beam path of the laser in order to process an area larger than the laser spot size. The number of pulses incident on the sample was controlled by the translation speed of the sample.

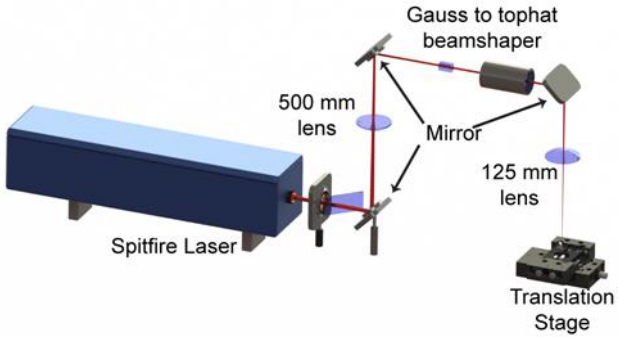

Fig.1 Schematic of the femtosecond laser surface processing (FLSP)

Tailoring Multiscale Surfaces

The size and shape of self-organized surface structures fabricated via FLSP are controlled through various fabrication parameters including the laser fluence, the number of laser shots per area incident on the sample, and the composition and pressure of the atmosphere during processing. The fluence and shot number are used as control parameters for determining the type of microstructure created on the surface. These parameters are two contrasting ways of controlling the total dose of the laser energy transferred to the substrate. To illustrate this, consider that a given amount of laser energy can be transferred to a target substrate either through a small number of laser pulses with a large fluence or through a large number of laser pulses with a small fluence. However, the laser fluence critically impacts the laser−matter interaction mechanisms attributed to the development of multiscale structures; we recently published a shot-by-shot study of the ability of the laser fluence to influence the physical formation mechanisms of the self-organized surface structures and utilized this control to fabricate multiscale metallic surface structures that rise above the original surface [27]. Thus, control of the laser dose via a calculated selection of both the laser fluence and the number of pulses on the sample is a convenient method to produce a range of unique surface morphologies.

The type of surface morphology that is created depends on the balance of the three main mechanisms that govern how the self-organized microstructures are formed. The three main mechanisms are preferential ablation, fluid flow, and material redeposition. These are depicted in Figure 2. The combination of these three mechanisms defines the properties and geometry of the self-organized microstructures. These mechanisms are controlled by changing the fluence and shot combination. A detailed description of the development and formation of these structures is beyond the scope of this paper; a more detailed description is provided by Zuhlke, et al [27].

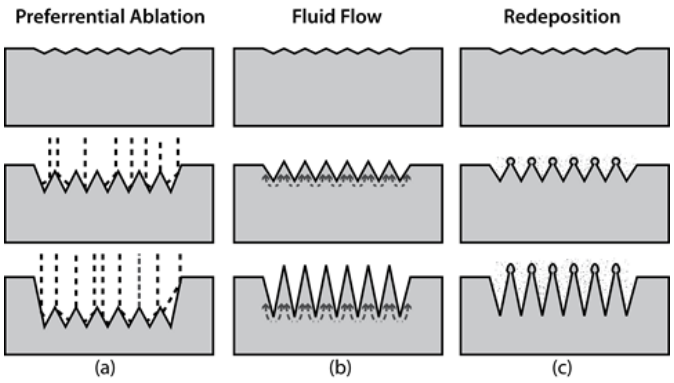

Fig.2 Schematic illustrations of three growth mechanisms leading to the development of multiscale surface features from surface precursor sites upon laser irradiation. (a) Material is ablated away around a scattering site to form structures. (b) Material is melted and flows to form structures. (c) Particles are redeposited to form structures.

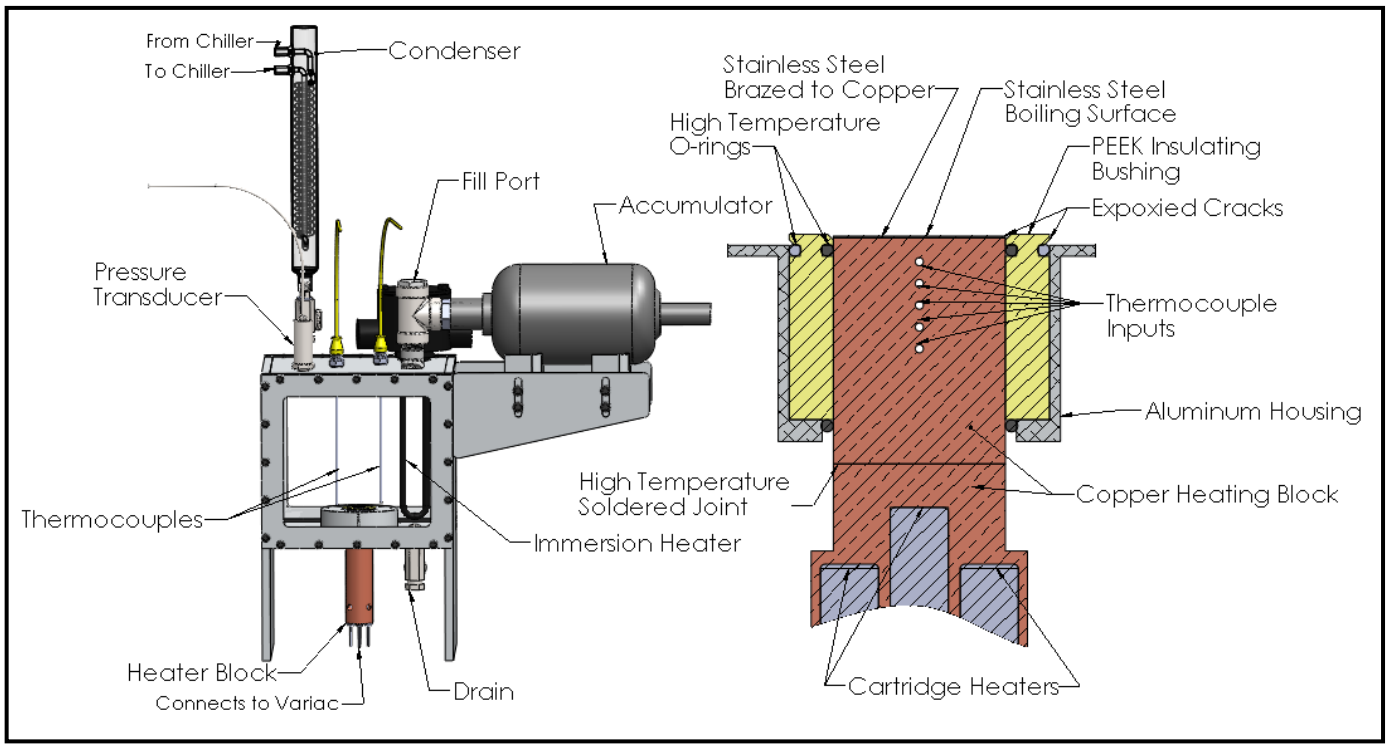

Fig. 3 Left – Full experimental pool boiling setup, Right – Cross sectional view of heating block and boiling surface

Pool Boiling Experimental Setup and Procedure

A closed system pool boiling experimental setup was used for the experimental procedures. This setup is highlighted in Figure 3. The test rig was designed to accommodate a variety of working fluids. For the presented results, deionized water was used as the working fluid. The test rig was filled with eight liters of deionized water. The system was brought to the saturation temperature of the water by the use of an immersion heater (Omega - MT-112E2/120V) controlled by an analog variac. The water temperature and internal pressure were monitored with the use of two K-type thermocouples (Omega - M12KIN-18-U-6-D) and a pressure transducer (Omega - MMA100V5P4C0T4A5CE) that were connected to LabVIEW. The water was degassed for a half hour before measurements were taken. The steam produced was directed through a coil condenser (Quark Glass - qc-6-4sp) that was vented to the atmosphere. The condenser was supplied with cold water with the use of a chiller. The test rig also includes a bladder accumulator for regulating the environment pressure. This was not used for this experiment due to all measurements being taken at atmospheric pressure. Two Lexan view windows were incorporated into the test rig to allow flow visualization.

Once the system was allowed to reach the saturation temperature of the water, the boiling surface heater was turned on. The boiling surface was heated with the use of a copper heating block containing five cartridge heaters (Omega - CSH-203450/120V). These cartridge heaters were controlled with an analog variac. This copper heating block was attached to the upper copper heating block (see Fig. 3) with the use of a high temperature solder (McMaster - 7685A12). The upper copper heating block has five thermocouple holes drilled to the center of the block. These thermocouples were used to measure the temperature gradient within the block and calculate the heat flux. These thermocouple locations were spaced 0.125” apart. These thermocouples were used with LabVIEW to monitor and calculate the heat flux as well as interpolate the surface temperature. Heat flux values were recorded after the system had reached steady state and the temperature profiles shown in LabVIEW were horizontal. The actual boiling surface exposed to the water was made from a 304 stainless steel wafer. This wafer was 1.0” in diameter and had a thickness of 0.010” inches. This wafer was brazed onto the upper copper heating block to ensure an efficient contact between the two. The two dissimilar materials were brazed with a silver solder paste (Muggyweld - SSQ-6). The surface temperature was interpolated with the use of measured temperature gradient. The thermal conductivity of copper was assumed to be constant at 400 W/mK while the thermal conductivity of the stainless steel wafer was assumed to vary linearly with temperature. The contact resistance between the copper and stainless steel was neglected due to the highly conductive silver solder braze used.

A high temperature PEEK plastic insulating bushing was used to insulate the upper copper heating block. Fiberglass insulation was used to insulate the lower copper heating block (not pictures in Fig. 3). High temperature silicon o-rings were used to seal between the concentric heating and insulating pieces. To ensure that nucleation would not initially occur on the outer edges of the boiling surface, a special epoxy was used for bonding dissimilar materials (Mcmaster - 7513A1).

Surface Characterization

In the current experiment two surfaces were tested and compared for boiling heat transfer performance. A polished

stainless steel surface and a laser processed surface tested and compared. The polished stainless steel sample was polished to a mirror finish through the use of a series of buffing compounds. The laser processed surface was fabricated to have a self-organized mound like micro structure with a layer of nanoparticles covering the mound structures.

Several machines were used to characterize each surface. A Rame-Hart Model 590 F4 Series Goniometer and Tensiometer was used to measure the contact angle of both the polished and processed sample. Deionized water was used for this measurement. The contact angle of the polished surface was found to be approximately 80°. The FLSP process results in a porous surface layer due to the dense layer of nanoparticles that layer the microstructures [28]. This porous layer results in a surface that has high wicking capabilities. This results in a contact angle of nearly zero. An attempt to measure the contact angle of the processed surface was made, but the machine was unable to give an accurate measurement. The processed surface was so superwicking that when a droplet was placed onto it the surface it would completely flatten and wick across the surface. This made an actual measurement very difficult. Because of this the contact angle was determined to be zero.

In order to characterize the processed surface two methods were used. SEM imaging and Laser-confocal surface profilometry. The results from these methods are shown in Figure 4. The SEM images show the self-organized nature of the mound like microstructures. These mound structures are covered in a layer of nanoparticles that can be seen in part B of Figure 4. These nanoparticles blanket the microstructures and form lines and ridges across each microstructure. These nanoparticles produce the porous layer above the microstructure. In our previous work, TEM imaging was used to view a cross section of the microstructure and measure the nanoparticle layer [28]. It was found that the nanoparticle layer was responsible for a significant portion of the total microstructure height. The nanoparticle layer was measured to be up to 4.6 µm thick which was around 1/3 of the total microstructure height. The TEM images also show the porous nature of the nanoparticle layer.

Finally the laser-confocal microscope was used to create a 3D profile of the surface as well as take physical measurements. The 3D surface generated can be seen in part C of Figure 4. From this measurement the maximum height, average height, surface roughness, and surface area ratio were determined. The maximum height of the microstructure was found to be around 43 µm. It can be seen from the images in Figure 4 that very deep pits form around the mound structures. The average peak to valley height of the microstructures was found to be around 23 µm tall. The surface area ratio, which is defined as the ratio of total surface area divided by the cross sectional planar surface area, was found to 4.5. The rms surface roughness was measured to be 6.4 µm.

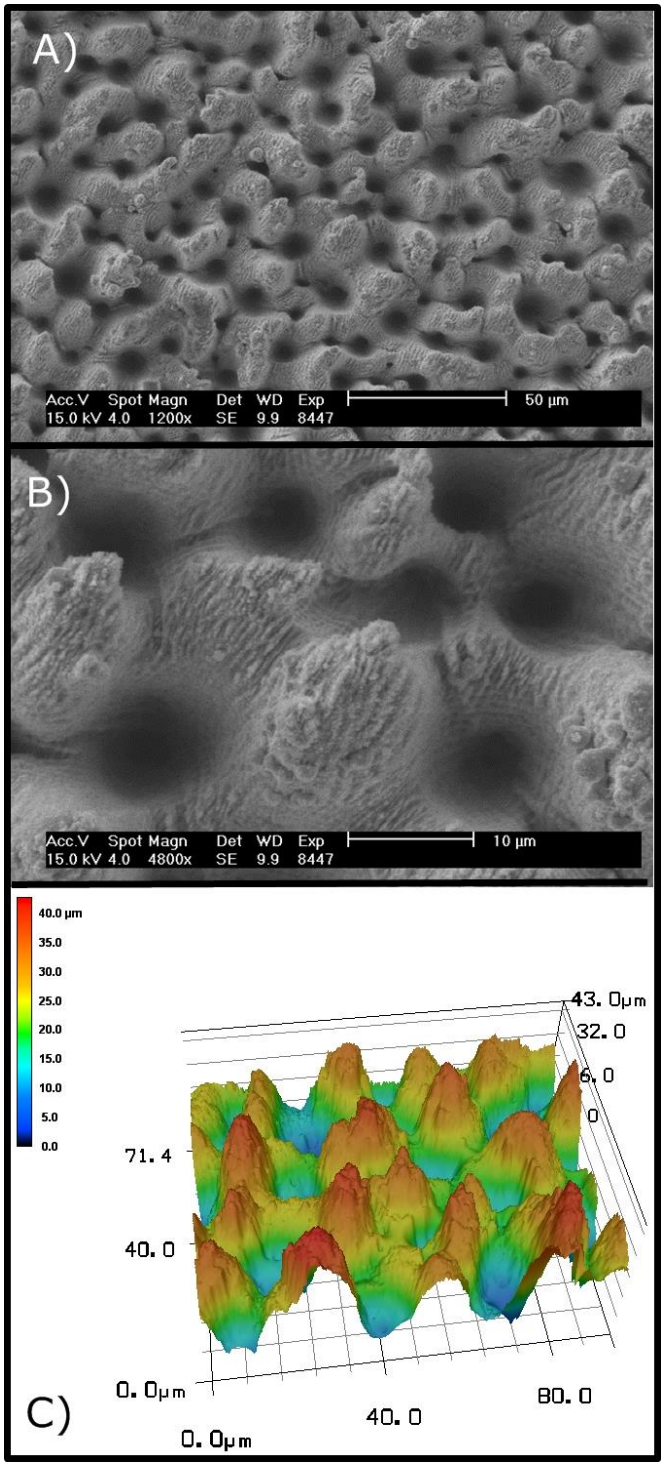

Fig. 4 SEM and laser confocal microscope images of the femtosecond laser processed surface. A) SEM magnification of 1200x and scale bar of 50 µm, B) SEM image magnification of 4800x and scale bar of 10 µm, C) Laser confocal 3D generated image.

RESULTS

For each of the two sample surfaces tested, measurements were first taken at low heat fluxes and then slowly increased until the critical heat flux was attained. The results are shown in Figure 5. It can be seen from this figure that there was a

drastic difference between the two surfaces. The processed surface consistently outperformed the polished sample at every surface temperature. The polished sample was found to have a critical heat flux of 91 W/cm^2 at a surface temperature of 39.8 °C. At this temperature and the heat flux the heat transfer coefficient was found to be 22,800 W/m^2. The processed surface was found to have a critical heat flux of 122 W/cm^2 at a surface temperature of 18.1 °C. This heat flux and surface temperature combination resulted in a heat transfer coefficient of 67,400 W/m^2. The processed surfaced resulted in a maximum HTC that was around 7.5 times greater than the HTC of the polished surface at the same surface temperature. This shift in the boiling curve to the left is very advantageous for most applications. This allows for a large amount of heat to be transferred at relatively cool surface temperatures. The steep slope of the curve is also advantageous because of the relatively small surface temperature change (around 10 °C). This small temperature change at varying heat fluxes is beneficial for applications that see rapidly changing heat transfer demands. A laser processed surface could help prevent heat transfer surface failures due to thermal fatigue.

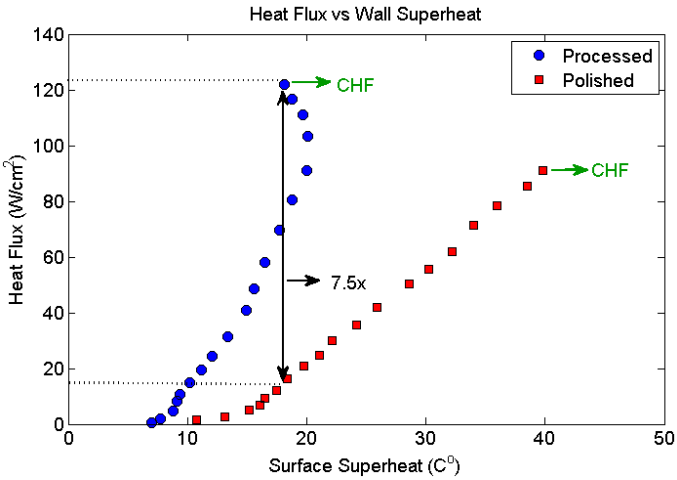

Fig. 5 Heat fluxes with respect to surface temperature for both the laser processed and polished stainless steel surfaces.

As expected from the data shown in Figure 5, the two surfaces displayed very different visual boiling characteristics. These can be seen in Figure 6. Bubble nucleation was first observed at around 10 °C of superheat for the polished sample. Nucleation typically started in the center of the surface but also was found at the edges of the sample. Epoxy was applied the edges of the sample in order to limit this unwanted nucleation. At low heat fluxes on a few nucleation sites were active. These active sites produced large bubbles that were slow to detach from the surface. From Figure 6 the polished sample depicts the nucleation at the early stages of the boiling curve. This nucleation image was taken at a surface temperature of around 13 °C and a heat flux of around 3 W/cm^2

As for the processed sample, the nucleation appeared much different. First, the onset of nucleation occurred at a much lower temperature than the polished sample. This occurred at a temperature of 7 °C. At this temperature there was also nearly zero nucleation at the edges of the sample like the polished surface. This means that the micro/nanostructures created a more favorable nucleation site than the crack found between the epoxy and surface transition. Also at the onset of nucleation, there were significantly more active nucleation sites. These active sites also produced very small bubbles that quickly formed and detached from the surface. In Figure 6 the early stages of nucleation are shown for the laser processed surface. This image was taken at a surface temperature of 7.7 °C and a heat flux of 2 W/cm^2.

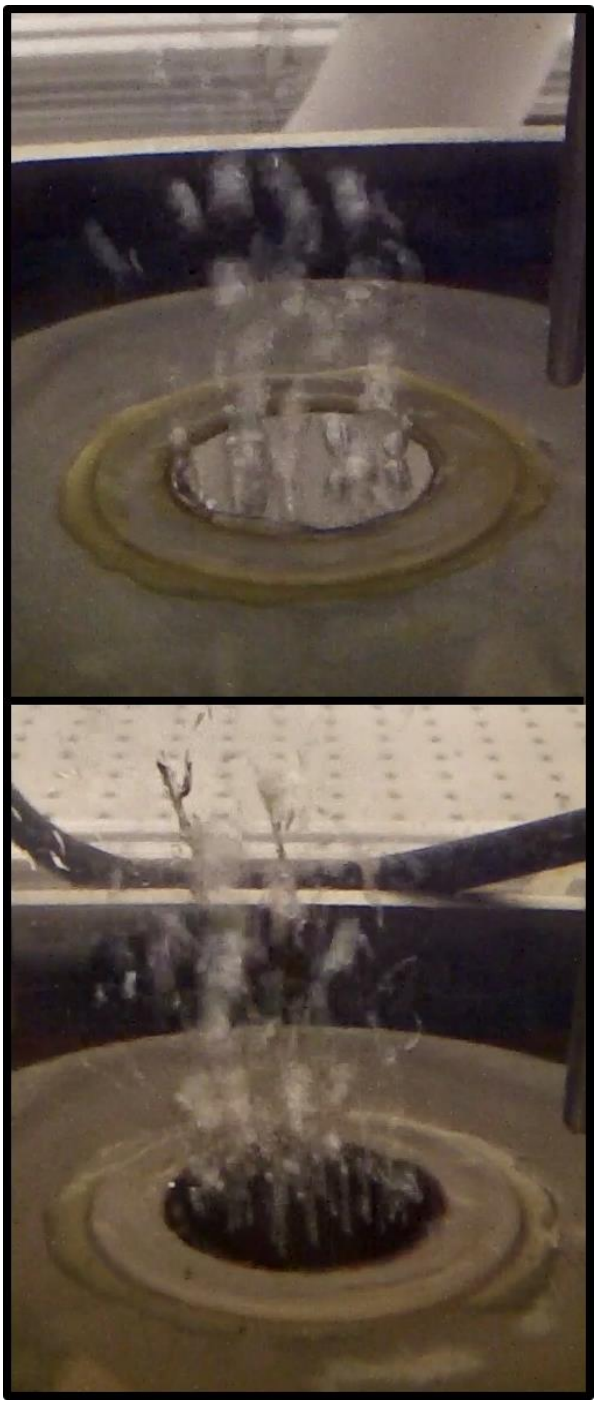

Fig. 6 Onset of boiling nucleation for both heat transfer surfaces: Top – polished sample, 13 °C superheat and 3 W/cm^2, Bottom – processed sample, 7.7 °C and 2 W/cm^2

As can be seen from both Figure 5 and 6, the femtosecond laser surface processing technique has a significant effect on the boiling performance of a stainless steel heat transfer surface. This process creates a unique hierarchal structure consisting of mounds covered in a dense layer of porous nanoparticles. This combination results in a surface with a very low contact angle and high wicking capabilities. This combination prevents the onset of film boiling by maintaining the liquid solid contact at high heat fluxes. This results in the achievement of a higher critical heat flux. The femtosecond laser surface process also creates a very rough surface. The microstructures produce an increased surface area ratio while the nanoparticle coating creates an abundance of potential nucleation sites. This combination results in more heat transfer surface area exposed to the liquid as well a more efficient nucleation process. This is why the laser processed surface results in such a drastic improvement of the heat transfer coefficient.

The femtosecond laser surface process is a very efficient way of creating a hierarchal micro/nanostructure on nearly any metallic surface, especially a stainless steel surface. This method creates the microstructure from the base material and thus creates a very robust microstructure that is beneficial for industry applications. The results reported for this processed surface are our group's initial efforts at creating an enhanced functionalized surface for boiling heat transfer. The performance of the processed stainless steel is very comparable and/or better than current methods of enhancing metallic heat transfer surfaces [10], [11]. With some additional experiments and surface variations it is believed that this surface enhancement technique will be comparable to any microfabrication technique.

CONCLUSION

Through the use of a femtosecond laser surface process (FLSP) a stainless steel surface was fabricated with a hierarchal micro/nanostructure. This structure consists of a mound like microstructure that is coated with a dense layer of nanoparticles. The enhancement of the surface results in a superwicking surface with an augmented surface area and increase in potential nucleation sites. From the experimental results it was shown that this laser processing technique was able to increase the critical heat flux of the stainless steel sample from 91 to 122 W/cm^2 while also increasing the heat transfer coefficient by nearly 7.5 times to a value of 67,400 W/m^2. This method of surface enhancement is unique in that it creates the micro/nanostructure with the base material and thus is capable of producing a robust and permanent surface modification on nearly any metallic surface. With further research and development of these structures it is possible to create surfaces with heat transfer capabilities that are comparable or better than any microfabrication technique and can easily be applied for large scale applications.

ACKNOWLEDGMENT

This work has been supported by a grant through the Nebraska Center for Energy Sciences Research (NCESR) with funds provided by Nebraska Public Power District (NPPD) to the University of Nebraska – Lincoln (UNL) No. 4200000844, by funds from the Air Force Research Laboratory (AFRL) High Energy Laser-Joint Technology Office (HEL-JTO) No. FA9451-12-D-019/0001, JTO Number: 12-BAA-0467, and by funds from the Department of Mechanical and Materials Engineering and the College of Engineering at UNL, awarded to SN.

REFERENCES

[1] S. Kim, H. D. Kim, H. Kim, H. S. Ahn, H. Jo, J. Kim, and M. H. Kim, "Effects of Nano-Fluid and Surfaces with Nano Structure on the Increase of CHF," Exp. Therm. Fluid Sci., vol. 34, no. 4, pp. 487–495, May 2010.

[2] K.-H. Chu, R. Enright, and E. N. Wang, "Structured Surfaces for Enhanced Pool Boiling Heat Transfer," Appl. Phys. Lett., vol. 100, no. 24, p. 241603, 2012.

[3] Z. Yao, Y.-W. Lu, and S. G. Kandlikar, "Micro/nano Hierarchical Structure in Microchannel Heat Sink for Boiling Enhancement," in *2012 IEEE 25th International Conference on Micro Electro Mechanical Systems (MEMS)*, 2012, pp. 285–288.

[4] A. R. Betz, J. Jenkins, C.-J. "Cj" Kim, and D. Attinger, "Boiling Heat Transfer on Superhydrophilic, Superhydrophobic, and Superbiphilic Surfaces," Int. J. Heat Mass Transf., vol. 57, no. 2, pp. 733–741, Feb. 2013.

[5] A. R. Betz, J. Xu, H. Qiu, and D. Attinger, "Do Surfaces with Mixed Hydrophilic and Hydrophobic Areas Enhance Pool Boiling?," Appl. Phys. Lett., vol. 97, no. 14, p. 141909, 2010.

[6] Z. Yao, Y.-W. Lu, and S. G. Kandlikar, "Effects of Nanowire Height on Pool Boiling Performance of Water on Silicon Chips," Int. J. Therm. Sci., vol. 50, no. 11, pp. 2084–2090, Nov. 2011.

[7] M.-C. Lu, R. Chen, V. Srinivasan, V. P. Carey, and A. Majumdar, "Critical Heat Flux of Pool Boiling on Si Nanowire Array-Coated Surfaces," Int. J. Heat Mass Transf., vol. 54, no. 25–26, pp. 5359–5367, Dec. 2011.

[8] R. Chen, M.-C. Lu, V. Srinivasan, Z. Wang, H. H. Cho, and A. Majumdar, "Nanowires for Enhanced Boiling Heat Transfer.," Nano Lett., vol. 9, no. 2, pp. 548–53, Feb. 2009.

[9] H. S. Ahn, C. Lee, J. Kim, and M. H. Kim, "The Effect of Capillary Wicking Action of Micro/nano Structures on Pool Boiling Critical Heat Flux," Int. J. Heat Mass Transf., vol. 55, no. 1–3, pp. 89–92, Jan. 2012.

[10] B. Feng, K. Weaver, and G. P. Peterson, "Enhancement of Critical Heat Flux in Pool Boiling Using Atomic Layer Deposition of Alumina," Appl. Phys. Lett., vol. 100, no. 5, p. 053120, 2012.

[11] T. J. Hendricks, S. Krishnan, C. Choi, C.-H. Chang, and B. Paul, "Enhancement of Pool-Boiling Heat Transfer Using Nanostructured Surfaces on Aluminum and Copper," Int. J. Heat Mass Transf., vol. 53, no. 15–16, pp. 3357–3365, Jul. 2010.

[12] P. Bizi-Bandoki, S. Benayoun, S. Valette, B. Beaugiraud, and E. Audouard, "Modifications of

Roughness and Wettability Properties of Metals Induced by Femtosecond Laser Treatment," Appl. Surf. Sci., vol. 257, no. 12, pp. 5213–5218, Apr. 2011.
[13] Z. K. Wang, H. Y. Zheng, and H. M. Xia, "Femtosecond Laser-Induced Modification of Surface Wettability of PMMA for Fluid Separation in Microchannels," Microfluid. Nanofluidics, vol. 10, no. 1, pp. 225–229, Jul. 2010.
[14] J. Wu, J. Xia, W. Lei, and B. Wang, "A One-Step Method to Fabricate Lotus Leaves-Like ZnO Film," Mater. Lett., vol. 65, no. 3, pp. 477–479, Feb. 2011.
[15] T. Baldacchini, J. E. Carey, M. Zhou, and E. Mazur, "Superhydrophobic Surfaces Prepared by Microstructuring of Silicon Using a Femtosecond Laser.," Langmuir, vol. 22, no. 11, pp. 4917–9, May 2006.
[16] C. H. Crouch, J. E. Carey, J. M. Warrender, M. J. Aziz, E. Mazur, and F. Y. Génin, "Comparison of Structure and Properties of Femtosecond and Nanosecond Laser-Structured Silicon," Appl. Phys. Lett., vol. 84, no. 11, p. 1850, 2004.
[17] S. I. Dolgaev, S. V. Lavrishev, a. a. Lyalin, a. V. Simakin, V. V. Voronov, and G. a. Shafeev, "Formation of Conical Microstructures Upon Laser Evaporation of Solids," Appl. Phys. A Mater. Sci. Process., vol. 73, no. 2, pp. 177–181, Aug. 2001.
[18] K. Koch, B. Bhushan, Y. C. Jung, and W. Barthlott, "Fabrication of Artificial Lotus Leaves and Significance of Hierarchical Structure for Superhydrophobicity and Low Adhesion," Soft Matter, vol. 5, no. 7, p. 1386, 2009.
[19] E. Stratakis, a Ranella, and C. Fotakis, "Biomimetic Micro/nanostructured Functional Surfaces for Microfluidic and Tissue Engineering Applications.," Biomicrofluidics, vol. 5, no. 1, p. 13411, Jan. 2011.
[20] B. Tull, J. Carey, and E. Mazur, "Silicon Surface Morphologies after Femtosecond Laser Irradiation," Mrs …, vol. 31, no. August, pp. 626–633, 2006.
[21] B. Wu, M. Zhou, J. Li, X. Ye, G. Li, and L. Cai, "Superhydrophobic Surfaces Fabricated by Microstructuring of Stainless Steel Using a Femtosecond Laser," Appl. Surf. Sci., vol. 256, no. 1, pp. 61–66, Oct. 2009.
[22] B. K. Nayak, M. C. Gupta, and K. W. Kolasinski, "Spontaneous Formation of Nanospiked Microstructures in Germanium by Femtosecond Laser Irradiation," Nanotechnology, vol. 18, no. 19, p. 195302, May 2007.
[23] B. K. Nayak and M. C. Gupta, "Ultrafast Laser-Induced Self-Organized Conical Micro/nano Surface Structures and Their Origin," Opt. Lasers Eng., vol. 48, no. 10, pp. 966–973, Oct. 2010.
[24] T.-H. Her, R. J. Finlay, C. Wu, and E. Mazur, "Femtosecond Laser-Induced Formation of Spikes on Silicon," Appl. Phys. A Mater. Sci. Process., vol. 70, no. 4, pp. 383–385, Apr. 2000.
[25] T. Yong Hwang and C. Guo, "Polarization and Angular Effects of Femtosecond Laser-Induced Conical Microstructures on Ni," J. Appl. Phys., vol. 111, no. 8, p. 083518, 2012.
[26] A. Y. Vorobyev and C. Guo, "Direct Femtosecond Laser Surface Nano/microstructuring and Its Applications," Laser Photon. Rev., vol. 7, no. 3, pp. 385–407, May 2013.
[27] C. Zuhlke, T. Anderson, and D. Alexander, "Formation of Multiscale Surface Structures on Nickel via Above Surface Growth and Below Surface Growth Mechanisms Using Femtosecond Laser Pulses," Opt. Express, vol. 21, no. 7, pp. 97–98, 2013.
[28] C. Kruse, T. Anderson, C. Wilson, C. Zuhlke, D. Alexander, G. Gogos, and S. Ndao, "Extraordinary Shifts of the Leidenfrost Temperature from Multiscale Micro/nanostructured Surfaces.," Langmuir, vol. 29, no. 31, pp. 9798–806, Aug. 2013.

.